Aerosol characterization of the stratospheric plume from the volcanic eruption at Hunga Tonga January 15th 2022

Corinna Kloss[1], Pasquale Sellitto[2], jean-baptiste renard[3], Alexandre Baron[4], Nelson BEGUE[5], Bernard Legras[6], Gwenael Berthet[7], Emmanuel Briaud[7], Elisa Carboni[8], Clair Duchamp[6], Valentin Duflot[9], Patrick Jacquet[7], Nicolas Marquestaut[10], Jean-Marc Metzger[11], Guillaume Payen[11], Marion Ranaivombola[12], Tjarda Roberts[3], Richard Siddans[13], and Fabrice Jegou[14]

[1]Laboratoire de Physique et Chimie de l'Environment et de l'Espace (LPC2E), CNRS
[2]Laboratoire Interuniversitaire des Systèmes Atmosphériques (LISA-IPSL)
[3]CNRS
[4]University of La Réunion
[5]Laboratoire de l'atmosphere et des Cyclones-Universite de la Reunion
[6]Ecole Normale Superieure
[7]French National Centre for Scientific Research (CNRS)
[8]University of Oxford
[9]LACy UMR8105/OSUR
[10]Observatoire des Sciences de l'Univers de La Réunion
[11]OSUR
[12]Laboratoire de l'Atmosphere et des Cyclones-Université de la Reunion
[13]Rutherford Appleton Laboratory
[14]LPC2E / French National Centre for Scientific Research (CNRS)

November 21, 2022

Abstract

Following the Hunga Tonga eruption (20.6°S, 175.4°W, mid-January 2022), we present a balloon-borne characterization of the stratospheric aerosol plume one week after its injection (on 23 and 26/01/2022, La Réunion island at 21.1°S, 55.3°E). Satellite observations show that flight #1 took place during the overpass of a denser plume of sulfate aerosols (SA) compared to a more diluted plume during flight #2. Observations show that the sampled plumes (at around 22, 25 and 19 km altitude, respectively) consist exclusively of very small particles (with radius < 1 µm). Particles with radii between 0.5 and 1.0 µm show optically transparent features pointing to predominant SA. Particles with radii below 0.5 µm are partly absorbing, which could point to small sulfate coated ash particles, a feature not identified with space-borne observations. This shows that in situ observations are necessary to fully characterize the microphysical properties of the plumes tracked by space-borne instruments.

Aerosol characterization of the stratospheric plume from the volcanic eruption at Hunga Tonga January 15^{th} 2022

Corinna Kloss [1], Pasquale Sellitto [2,3], Jean-Baptiste Renard [1], Alexandre Baron [4], Nelson Bègue [4], Bernard Legras [5], Gwenaël Berthet [1], Emmanuel Briaud [1], Elisa Carboni [6], Clair Duchamp [5], Valentin Duflot [4], Patrick Jacquet [1], Nicolas Marquestaut [7], Jean-Marc Metzger [7], Guillaume Payen [7], Marion Ranaivombola [4], Tjarda Roberts [1], Richard Siddans [6], Fabrice Jégou [1]

[1]Laboratoire de Physique et Chimie de l'Environnement et de l'Espace, CNRS/Université d'Orléans, UMR 7328
[2]Univ. Paris Est Créteil and Université de Paris-Cité, CNRS, Laboratoire Interuniversitaire des Systèmes Atmosphériques (LISA-IPSL), Institut Pierre Simon Laplace
[3]Istituto Nazionale di Geofisica e Vulcanologia, Osservatorio Etneo
[4]Laboratoire de l'Atmosphère et des Cyclones (LACy, UMR 8105 CNRS, Université de la Réunion, Météo-France), Université de La Réunion
[5]Laboratoire de Météorologie Dynamique, ENS-PSL/ Sorbonne Université/ École Polytechnique, UMR CNRS 8539
[6]UK Research and Innovation, Science and Technology Facilities Council, Rutherford Appleton Laboratory
[7]Observatoire des Sciences de l'Univers de La Réunion, UAR 3365 (CNRS, Université de La Réunion, Météo-France)
[1]Orléans, France
[2]Créteil, France
[3]Catania, Italy
[4]97400 Saint-Denis de La Réunion, France
[5] Paris, France
[6]Chilton, UK
[7]97490, Saint-Denis de La Réunion, France

Key Points:

- Predominant particle size range of <1 μm within the stratospheric aerosol plume of the Hunga Tonga eruption.
- Optically absorbing particles within the plume for particles <0.5 μm point to fractured, very small ash particles.
- Mostly optically semi-transparent particles, for particle sizes between 0.5 and 1.0 μm result from small sulfur coated ash particles.

Corresponding author: Corinna Kloss, corinna.kloss@cnrs-orleans.fr

Abstract

Following the Hunga Tonga eruption (20.6°S, 175.4°W, mid-January 2022), we present a balloon-borne characterization of the stratospheric aerosol plume one week after its injection (on 23 and 26/01/2022, La Réunion island at 21.1°S, 55.3°E). Satellite observations show that flight #1 took place during the overpass of a denser plume of sulfate aerosols (SA) compared to a more diluted plume during flight #2. Observations show that the sampled plumes (at around 22, 25 and 19 km altitude, respectively) consist exclusively of very small particles (with radius < 1 μm). Particles with radii between 0.5 and 1.0 μm show optically transparent features pointing to predominant SA. Particles with radii below 0.5 μm are partly absorbing, which could point to small sulfate coated ash particles, a feature not identified with space-borne observations. This shows that in situ observations are necessary to fully characterize the microphysical properties of the plumes tracked by space-borne instruments.

Plain Language Summary

The Hunga Tonga-Hunga Ha'apai volcano (at 20.6°S, 175.4°W) erupted on 13/01 and 15/01/2022 with injection of gases and aerosols up to 55 km altitude. Here, we present a study based on in situ aerosol observations on weather balloons on La Réunion (21.1°S, 55.3°E) within the injected Hunga Tonga aerosol plume one week after the eruption (23/01/2022 and 26/01/2022). With respective satellite observations, we show that the first measurement flight took place during the overpass of a denser aerosol plume compared to the second flight. We find that the plume exhibits only small particles <1 μm, mainly consisting of sulfate aerosols (for particles between 0.5-1 μm in size) and an absorbing component for very small particles (<0.5 μm), possibly pointing to small ash particles coated by sulfur. This letter 'absorbing' feature is a unique contribution brought by in situ measurements that fills a gap left by space-borne instruments.

1 Introduction

The Hunga Tonga-Hunga Ha'apai (hereafter referred to as Hunga Tonga) volcano (20.57°S, 175.38°W) started an eruptive phase on 20/12/2021, with gas, steam and ash plumes periodically injected at around 12 km altitude. In mid-January larger eruptive events occurred on 13/01 and 15/01 (e.g. Yuen et al. (2022); Carr et al. (2022). The subaerial eruption on 13/01 started at 15:20 UTC, injected plumes into the stratosphere that were observed at altitudes as high as 20 km, with an estimated sulfur dioxide (SO_2) burden of 0.05 Tg (Witze, 2022). A larger, submarine, explosive eruption started on 15/01 at 04:02 UTC (Yuen et al., 2022), with an estimated SO_2 burden of 0.4-0.5 Tg (Witze, 2022). The CALIPSO-CALIOP (The Cloud-Aerosol Lidar and Infrared Pathfinder Satellite Observation) space LiDAR observed an aerosol plume with depolarizing properties at altitude of 38 km, on 15/01 (Sellitto et al., 2022). Stereoscopic geostationary observations suggest plume top altitudes of 50-55 km at 04:30 UTC (Carr et al., 2022; Proud et al., 2022) building a record altitude of any observed volcanic plume. The extraordinary nature of this eruption in terms of explosivity and subsequent injection altitude in the stratosphere, as well as large aerosol and water vapor in-plume contents (Sellitto et al., 2022), have immediately triggered vivid discussions and scientific exchange within the atmospheric community. We reactively organized a fast in situ measurement campaign for high-resolution aerosol observations within the injected plume to characterize the optical and microphysical composition of the plume. Here, we present in situ observations on the aerosol concentration and size distribution and corresponding analysis of the optical and microphysical properties of the aerosols within the stratospheric Hunga Tonga plume with the Light Optical Aerosol Counter (LOAC) on two balloon flights from OPAR (Observatoire de Physique de l'Atmosphère de la Réunion, 21.1°S and 55.3°E) on 23/01 and 26/01. At almost the same latitude and downwind of the Hunga Tonga plume's dispersion, OPAR is the ideal place for such early aerosol plume in situ investigations.

2 Methods

2.1 The LOAC balloon-borne optical counter

The Light Optical Aerosol Counter (LOAC) is an optical counter instrument that can be operated on weather balloons for observations in the stratosphere (Renard et al., 2016, 2020), with substantial improvements throughout its existence). For the described measurement flights, we used version 1.5 of the LOAC instrument with an improved optical chamber and sensitivity with a more powerful laser source compared to the previous version. LOAC provides measurements every ten seconds. For an increased signal to noise ratio, data are binned over an integration time of 20s. We use in situ measurement from LOAC on weather balloon flights from 23/01 (20:04-21:35 UTC) and 26/01 (17:24-19:54 UTC) at the Maïdo Observatory at La Réunion (21.1°S, 55.3°E). The LOAC instrument measures size-resolved aerosol concentration for particle sizes between 0.2 μm and ∼30 mm diameter (laser wavelength at 650 nm) distributed on 19 size classes. One outstanding feature of LOAC compared to other comparable instruments is the detection of scattered light at two angles (15 and 65° respective to the laser beam). This allows for a partial characterisation of the light absorbing properties and thus the typology of the observed aerosols (i.e. distinction between optically absorbing, semi-transparent and transparent solid particles, liquid, ice particles, (Renard et al., 2016). Aerosol extinction values stem from the conversion from measured aerosol concentration for size classes higher than 0.2 μm using Mie scattering theory and an estimate of the refractive index coming from the typology determination.

2.2 LiDAR observations at the Maïdo Observatory

LiDAR data used in this study are derived from observations conducted at the Maïdo Observatory, one of the three observation sites of the Atmospheric Physics Observatory of La Réunion (OPAR) located on Reunion Island (21.1°S, 55.3°E). The Maïdo Observatory is a permanent station, situated at 2160 m above mean sea level, for long term atmospheric observations (Baray et al., 2013). The used LiDAR system is the aerosol wing of the LIO3T (Duflot et al., 2017). The aerosol optical properties are retrieved following the Rayleigh slope method presented in Chazette et al. (1995). With a significant aerosol load between aerosol-free layers, it allows for conclusions on the aerosol optical thickness (AOT) of the plume. This constraint, as an input of an iterative Klett method (Klett, 1985) for the LiDAR inversion, enables to assess both the aerosol extinction coefficient and an average LiDAR ratio of the aerosol layer. The LiDAR ratio is the ratio of the extinction-to-backscatter coefficient and gives indications on some microphysical properties of the observed aerosols. According to Dieudonné et al. (2015) only the Lidar Ratios obtained during phases of aerosol extinction observation >0.02 km^{-1} are presented. The final temporal and vertical resolutions of the presented profiles are 5 min and 50 m, respectively.

2.3 IMS sulfate aerosols speciation and retrieval

The RAL (Rutherford Appleton Laboratory) Infra-red/Microwave Sounder (IMS) retrieval core scheme Siddans (2019) uses an optimal estimation (OE) spectral fitting procedure to retrieve atmospheric and surface parameters jointly from co-located measurements by IASI (Infrared Atmospheric Sounding Interferometer), AMSU (Advanced Microwave Sounding Unit) and MHS (Microwave Humidity Sounder) on MetOp spacecraft series, using RTTOV 12 (Radiative Transfer for TOVS) (Saunders et al., 2017) as the forward radiative transfer model. The use of RTTOV12 enables the retrieval of volcanic-specific aerosols (sulfate aerosol: SA) and trace gases (SO_2). The present paper uses IMS SA observations from its near-real time implementation (images can be viewed here: http://rsg.rl.ac.uk/vistool). The IMS scheme retrieves the optical depth of the SA at $\sim$1200 cm^{-1} (the peak of the mid-infrared extinction cross section, Sellitto and Legras (2016), assuming a Gaussian extinction coefficient profile shape peaking at 20 km altitude, with 2 km full-width-half-maximum. The bulk of the spectroscopic information on SA, in the IMS scheme, thus comes from the IASI Fourier transform spectrometer (Clerbaux et al., 2009), thus we will refer to these observations as IMS/IASI in the following.

3 Results

3.1 Transport of the Hunga Tonga plume above La Réunion island

To bring LOAC in situ observations in the larger scale context of the transported Hunga Tonga plume, we show the horizontal plume distribution with IMS SA optical depth observations in Figure 1. The first dispersion, removal of larger ash particles and rapid formation of SA has been shown by Sellitto et al. (2022), with the HIMAWARI Ash RGB recipe and CALIOP observations. An animation of MSG-1 brightness temperature observations (Da, 2015) with the Eumetrain RGB recipe (Eumetrain, 2020) is shown in the Supplementary Information (Movie S1 and Text S1, respectively) for an overview of the subsequent transport of the volcanic plume over the southern Indian Ocean. The RGB recipe allows for differentiations between water and ice clouds (grayish and shades of brown), ash (shades of red) and SO_2 and SA (shades of bright green). The spectral signatures of SO_2 and SA superpose in the spectral range covered by the RGB recipe and they cannot be readily disentangled without complementary information, as provided in Sellitto et al. (2017). In this case, greenish plumes are most likely an indication of SA-dominated plumes (Sellitto et al., 2022). The MSG-1 observations show a dense volcanic SA plume above La Réunion, starting from 21/01 and clearly visible until 23/01. During the night of the first LOAC observations (23/01, 20:04-21:35 UTC) the bulk SA plume had already moved to the South-West. The RGB MSG-1 analysis does not reveal a clear signature of transported ash from the Hunga Tonga eruption. However, the brightness temperature RGB retrieval is only sensitive to relatively high concentrations of ash or SA; low concentrations will therefore not clearly appear in the respective color on the map. For a more quantitative analysis of the plume, Figure 1 shows the horizontal distribution of the SA optical depth from IMS/IASI on 23/01 (Figure 1a) and 26/01 (Figure 1b), close in time to LOAC measurements during the night time overpass (at La Réunion at around 18:00 UTC, compared to LOAC observations 20:04-21:35 UTC for 23/01 and 17:24-19:54 UTC for 26/01). Consistently with what is observed with MSG-1 for SO_2/SA, IMS/IASI measurements suggest that the flight on 23/01 took place when a denser plume of SA was transported over La Réunion, compared to much diluted signatures for the flight on 26/01, where the later periphery of the main volcanic plume was overpassing La Réunion. Values of the thermal infrared SA optical depth as large as 0.05 are found for 23/01, pointing at a dense SA plume. The vertical aerosol extinction distribution of the aerosol plume at La Réunion, from the ground-based LIO3T observations at the Maïdo Observatory, is shown on the left side in Figure 2. These remote sensing observations are taken around the measurement time frame of LOAC in situ observations. Respective LOAC aerosol extinction observations at 532 nm (wavelength chosen according to LiDAR observations), observed during the indicated time frame (20:04-21:35 UTC), are shown on the right side (and in Figure S1). On 23/01 at 20:04-21:35 UTC LOAC observations (Figure 2a, right side and Figure S1) identify two main plume layers at around 22.6 and 24.9 km altitude, with peak values up to $\sim$4 10^{-3} km^{-1}. The LIO3T time series shows that LOAC observations were taken right before the arrival of a much denser section of the plume. With an average ascending speed of the balloon of 6 m/s in the stratosphere and a counting integration time of 20 seconds only a few measurement points originate from the plume. Peak aerosol extinction values between 22 and 23 km altitude

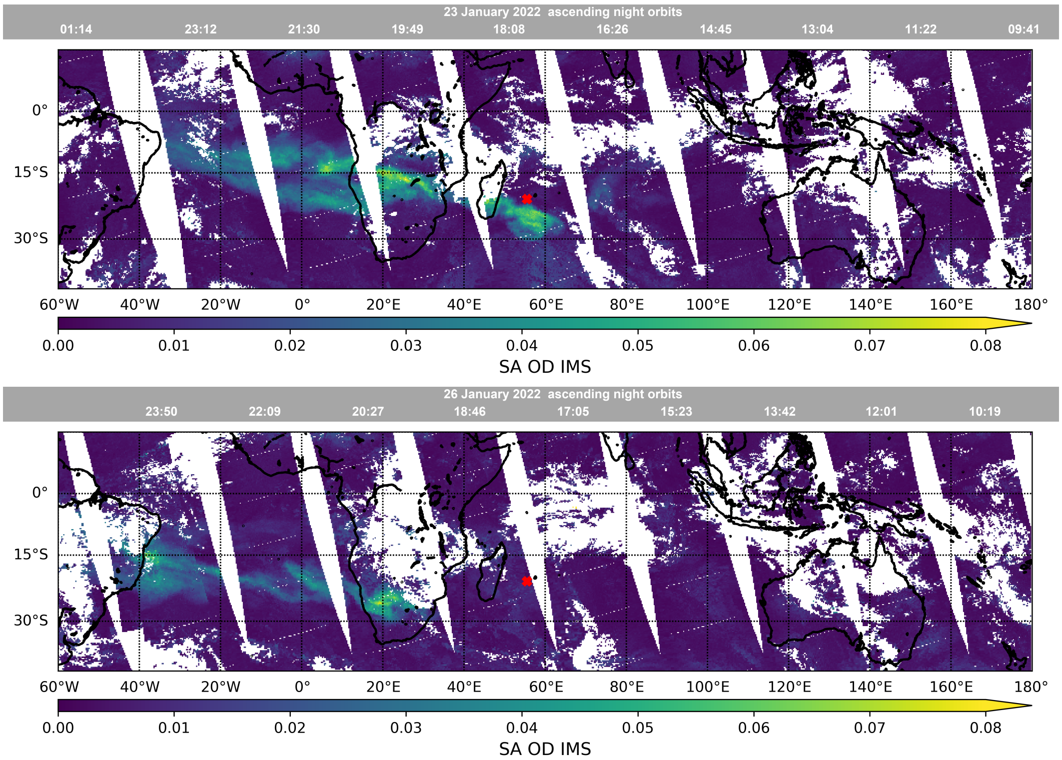

Figure 1. IMS/IASI SA optical depth observations with the respective timestamp of equator crossing in UTC (a) on 23/01 and (b) on 26/01. The red cross shows the location of LOAC measurement flights at La Réunion. Areas of no measurements and clouds are indicated in white.

from LIO3T observations during LOAC observations ($\sim$15 10^{-3} km^{-1}, with a LiDAR uncertainty of around 25 % at the plume's altitude) exceed LOAC aerosol extinction values ($\sim$3 10^{-3} km^{-1}) by a factor of 5. Multiple factors contribute to this observed difference: (a) The plume is likely not homogeneous in time and space and balloon observations with LOAC are not taken at the same position (at the plume altitude of 22.5 km, LOAC and LIO3T observations are 15.5 km apart), (b) LOAC observations do not consider particles with diameters below 200 nm and therefore represent a lower limit of the sampled plume. Large variations are expected within a heterogeneous plume and are expected to be the main reasons for the visible discrepancy.

During the time of the LOAC observations, LIO3T data do not show aerosol enhancements at 25 km altitude (at 25 km altitude LOAC was flying around 12 km further North compared to LIO3T observations). However, prior to LOAC observations a strong plume signal was observed at 25 km altitude for several hours to days (not shown here, LIO3T results will be published in more detail by Baron et al.). Furthermore, OMPS observations (Figure S2a) show the clear presence of an aerosol plume above La Réunion at around 10 UTC up to $\sim$27 km altitude, with peak values at $\sim$25 km. The respective stratospheric Aerosol Optical Depth of 0.12 (see Figure S2b) is significantly larger than LIO3T integrated optical depth observations, probably because of dense plume sections at lower stratospheric altitudes which are observed by OMPS but not by the ground LIO3T. The plume's evolution between the OMPS overpass and LOAC observations on 23/01 is presented in Figure S2c and d, respectively (light green shaded area). A LiDAR ratio of 68 $\pm$ 18 is observed within the peak aerosol plume. This is similar to what has previously been observed for volcanic plumes at 532 nm (Prata et al., 2017), but cannot be used to rule out the plume's composition and possible presence of ash, especially if diluted.

On 26/01 17:24-19:54 UTC, LOAC peak aerosol extinction values were observed at around 19.5 km altitude, with peak values at 0.4 10^{-3} km^{-1}. LIO3T observations show peak aerosol extinction values of up to 40 10^{-3} km^{-1} (around 100 times higher than LOAC observations), with a LiDAR uncertainty of about 50 % at the plume altitude (18-20 km). From the LIO3T time series, it becomes evident that the LOAC time frame took place during the end phase of the plume (peak phase) overpass at La Réunion. LiDAR observations detected a much denser plume, while LOAC missed the bulk of the plume, likely due to the same plume heterogeneity reasons as stated above. It is evident (from satellite and LIO3T observations) that the observations sample the same plume on 26/01 and 23/01, therefore we assume a similar plume composition. CALIOP aerosol backscatter data capture part of the same plume around 15° further West 3 h after LOAC observations at the same altitude range (see Figure S3 in the Supplementary Material).

3.2 Characterization of the plume's microphysical properties with in situ observations

Based on the general consistency of LOAC and LIO3T observations at La Réunion, we exploit the LOAC observations to derive the optical and microphysical properties of the Hunga Tonga plume. Aerosol size distribution observations from the two LOAC flights within and below the aerosol plume (as defined in Figure 2, right side and in Figure S1) are presented in Figure 3. Observed number concentrations for the two peak altitudes at 22 and 25 km on 23/01 exceed aerosol background concentrations at 20 km altitude by a factor of 10 to 40. One highlight result of LOAC observations is the clear identification of the aerosol size range within the Hunga Tonga plume. For the Pinatubo eruption (1991), for example a coarse mode of aerosol peak concentration for particles with radii > 1 μm was observed besides the typical concentration peak for radii < 1 μm (Deshler et al., 1993) and typically associated with coarse ash particles. For the Hunga Tonga aerosol plume, LOAC observations (measuring aerosol particles up to 30 μm) reveal the absence of such a second mode, i.e. plume particles radii exclusively remain below $\sim$1 μm (Figure 3a and b for the flights on 23/01 and 26/01, respectively). Such a monomodal fea-

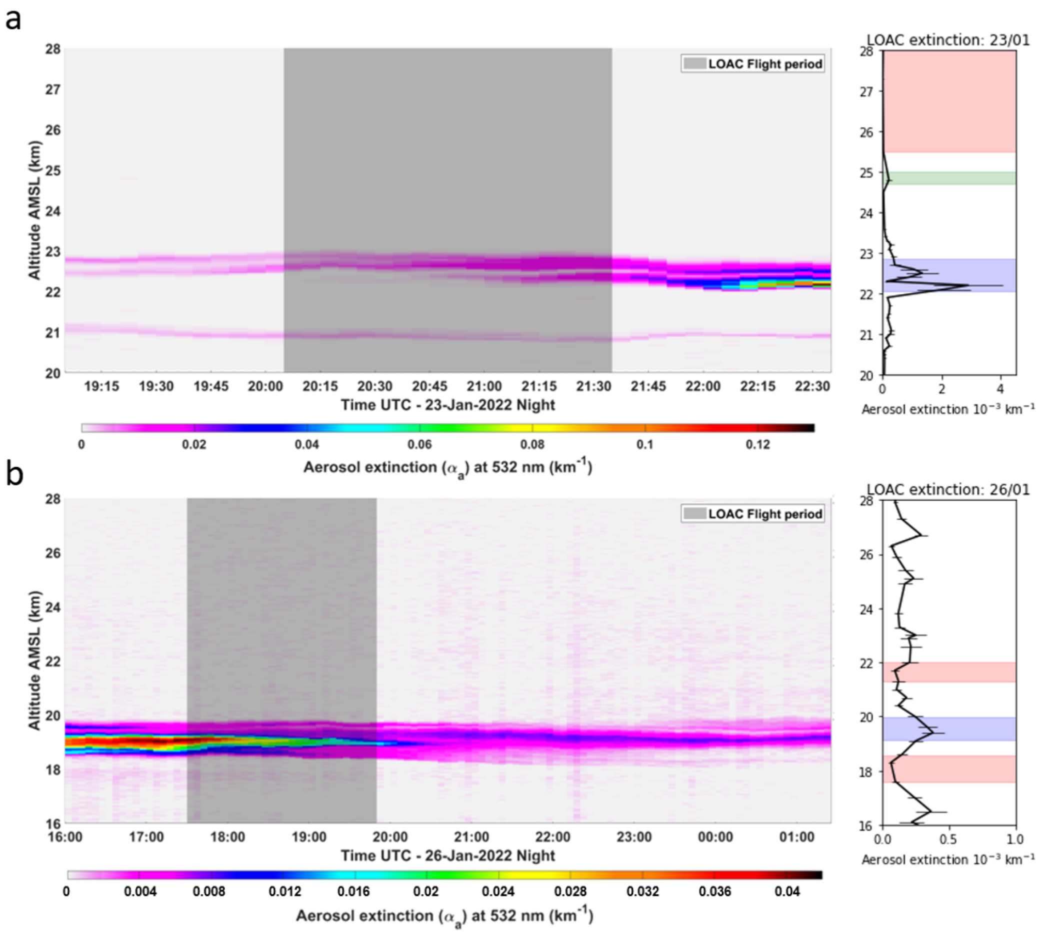

Figure 2. (Left) LIO3T aerosol observations at OPAR (La Réunion) at 532 nm wavelength for 23/01 (a) and 26/01 (b). The gray shaded blocks represent the timing of the LOAC in situ observations. (Right) Equivalent aerosol extinction at 532 nm, retrieved from LOAC aerosol concentration in situ observations with respective error bars. Horizontal shaded areas (also shown in the supplementary material in Figure S1) define altitude ranges used for further analysis (red: above/below plume, blue and green: in-plume).

Table 1. Aerosol typology within the Hunga Tonga plume at the altitude levels as defined in Figure 2 and Figure S1 in the supplementary material.

Flight	Particle size range	Typology
Jan 23rd lower peak (∼22 km)	< 0.5 μm	Transparent, Semi-transparent and Absorbing
	$0.5 - 1.0$ μm	Liquid
Jan 23rd upper peak (∼25 km)	< 0.5 μm	Semi-transparent
	$0.5 - 1.0$ μm	Transparent
Jan 26th	< 0.5 μm	Absorbing, Semi-transparent and Transparent
	$0.5 - 1.0$ μm	Transparent and Liquid

ture has already been observed e.g. for the Sarychev and Calbuco volcanic plumes from 2009 and 2015, respectively (Lurton et al., 2018; Bègue et al., 2017; Zhu et al., 2018).

LOAC typology particle classifications (optically absorbing, semi-transparent, transparent, liquid or ice particles) at the selected plume altitudes (as indicated in Figure 2) for the in situ observations are summarized in Table 1. For both measurement flights the aerosol plume forms a distinct layer of partly absorbing, semi-transparent particles for aerosol radii < 0.5 μm, and transparent, liquid particles for aerosol radii between 0.5 and 1.0 μm, at lower altitudes (around 22 km). The upper aerosol plume at 25 km altitude, measured on 23/01 shows a distinct layer of transparent (< 0.5 μm) and liquid (0.5-1.0 μm) particles. Aerosols at altitude levels outside the plumes (as defined in Figure 2 and S1) are purely identified as liquid aerosol particles by the LOAC typology retrieval. It is important to note that the partly absorbing component of the lower layer (∼22 km) is associated with very small particles (< 0.5 μm), which can explain why absorbing aerosols are not observed by satellites (that have reduced sensitivity to small particles). For example, Sellitto et al. (2022) identify plumes strongly dominated by SA, a few days after the UTLS injection, with satellite observations (e.g. OMPS, CALIOP). The observed absorbing component is not expected to have a significant impact on the larger scale optical/radiative properties of the plume. Finally, during both LOAC measurement flights ice particles were not identified.

4 Discussion

Based on LOAC plume observations on aerosol size distribution, concentration, and typology analysis we present possible aerosol compositions for the sampled Hunga Tonga plume.

One first overarching remark is that the Hunga Tonga plume exhibits very different microphysical features compared to the Pinatubo eruption of 1991, as well as more recent moderate stratospheric eruptions like Raikoke 2019 (Kloss et al., 2021), with a completely absent coarse ash aerosol mode. The Hunga Tonga plume (1-2 weeks after its eruption) is composed of very small particles. For all analyzed plume altitudes, the LOAC typology analysis consistently identifies liquid and transparent particles for particles of the size range $0.5 - 1.0$ μm. This points to the dominance of SA droplets within the plume. Sulfate aerosols are also consistently detected with satellite products (e.g. IMS/IASI SA optical depth). However, for all measured plumes (except 23/01 at 25 km altitude) the LOAC typology classification for particles with radii < 0.5 μm identifies absorbing and semi-transparent particles. This could point to partially small sulfate-coated ash particles or a thin, separated layer of ash below a layer of SA particles, with a ver-

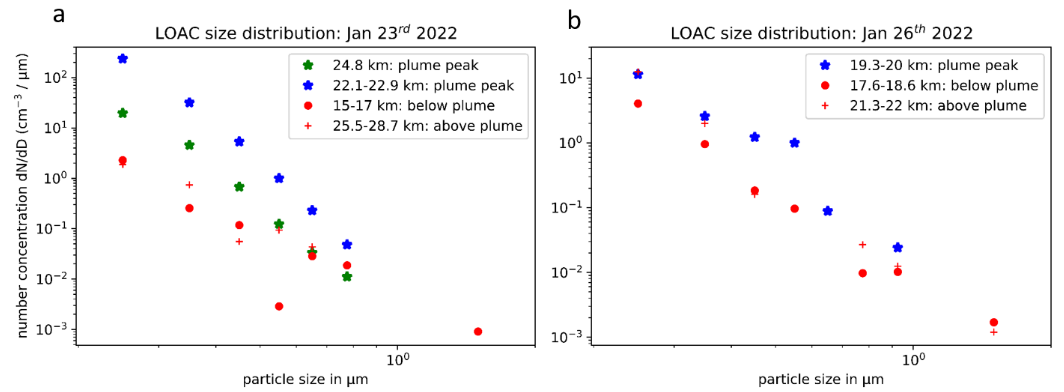

Figure 3. Observed aerosol size distribution at the identified aerosol plume heights as identified in Figure 1 and below the aerosol plume for the LOAC measurements from (a) 23/01 and (b) 26/01.

tical extent too thin to be identified as a separate layer by LOAC and space-borne observations. Such an ash-SA altitude separation was observed in Vernier et al. (2016) following the Kelud eruption in 2014. However, the absorbing particles observed by LOAC are exceptionally small (< 0.5 μm). For example 3 months after the Kelud eruption ash particles with radii exclusively above 0.5 μm were observed (Vernier et al., 2016). The exceptionally small ash particles in the Hunga Tonga plume could have originated from the particular eruption dynamics (magma-seawater interaction, Wylie et al. (1999) and (Yuen et al., 2022), with the inherent production of particularly small ash particles originating from the phreatomagmatic nature of the underwater Hunga Tonga eruption. The fact that satellite observations completely miss the small absorbing component of the sampled aerosol plume shows how valuable and important it is to not only rely on global-space-borne observations, but also to consider highly sensitive in situ observations with better spatial resolution.

The specific nature of the underwater eruption has produced record-breaking high stratospheric concentrations of water vapor with strong implications on aerosol formation and the stratospheric chemistry Sellitto et al. (2022). First results with the Microwave Limb Sounder and radio-sounding observations show the injection of exceptionally large water content into the stratosphere during the Hunga Tonga eruption (Khaykin et al., in preparation).

The plume measured at 25 km altitude on 23/01 shows a different composition compared to the plumes observed at 22 km. Particles of both size classes have a higher tendency towards optically transparent particles. This could point to a layer of predominant sulfate particles, clearly separating the plumes in terms of altitude and optical properties.

Overall, this study provides necessary, high resolution, complementary information to the existing and future studies on the microphysical properties of the plume, based on space-borne observations.

5 Open Research

LOAC in situ observations can be accessed from `https://daac.gsfc.nasa.gov/`. LiO3 observations are available at `https://geosur.osureunion.fr/geonetwork/srv/fre/catalog.search#/metadata/f2c35798-47b7-433c-8927-46cf7babca83`. For the access of the OMPS v 2.0 data are available at `https://disc.gsfc.nasa.gov/datasets/OMPS_NPP_LP_L2_AER_DAILY_2/summary` (NASA EarthData registration required). CALIOP and MSG-1 data are available at `https://www.icare.univ-lille.fr/asd-content/archive/?dir=CALIOP/` and `https://www.icare.univ-lille.fr/asd-content/archive/?dir=GEO/MSG+0415/L1_B/` (Free instantaneous registration on icare is required `https://www.icare.univ-lille.fr/asd-content/register`).

Acknowledgments

This study was supported by Le laboratoire d'excellence VOLTAIRE (VOLatils – Terre, Atmosphère et Interactions - Ressources et Environnement; ANR-10-LABX-100-01) and the ANR ASTUS (ANR-21-CE01-0007-01). The authors acknowledge the European Communities, the Région Réunion, CNRS, and Université de la Réunion for their support and contributions in the construction phase of the research infrastructure OPAR (Observatoire de Physique de l'Atmosphère de La Réunion). OPAR is presently funded by CNRS (INSU), Météo France and Université de La Réunion and managed by OSU-R (Observatoire des Sciences de l'Univers de La Réunion, UAR 3365). We would furthermore like to thank the whole scientific and technical team at OPAR responsible for LiDAR observations and help with LOAC balloon launches. We are grateful for the fast administrational arrangements at CNRS and University d'Orléans for the spontaneous campaign. Brian Kerridge at RAL is acknowledged for his help with the IMS product. We thank Virginie Lancelot and the OSUC- team for fast administrational realization of the financement and travel logistics.

References

Baray, J.-L., Courcoux, Y., Keckhut, P., Portafaix, T., Tulet, P., Cammas, J.-P., … Delmas, R. (2013). Maïdo observatory: a new high-altitude station facility at Reunion Island (21° S, 55° E) for long-term atmospheric remote sensing and in situ measurements. *Atmospheric Measurement Techniques*, *6*(10), 2865–2877. Retrieved from https://amt.copernicus.org/articles/6/2865/2013/ doi: 10.5194/amt-6-2865-2013

Bègue, N., Vignelles, D., Berthet, G., Portafaix, T., Payen, G., Jégou, F., … Godin-Beekmann, S. (2017). Long-range transport of stratospheric aerosols in the Southern Hemisphere following the 2015 Calbuco eruption. *Atmospheric Chemistry and Physics*, *17*(24), 15019–15036. Retrieved from https://acp.copernicus.org/articles/17/15019/2017/ doi: 10.5194/acp-17-15019-2017

Carr, J. L., Horváth, k., Wu, D. L., & Friberg, M. D. (2022). Stereo Plume Height and Motion Retrievals for the Record-Setting Hunga Tonga-Hunga Ha'apai Eruption of 15 January 2022. *Geophysical Research Letters*, *49*(9), e2022GL098131. Retrieved from https://agupubs.onlinelibrary.wiley.com/doi/abs/10.1029/2022GL098131 (e2022GL098131 2022GL098131) doi: https://doi.org/10.1029/2022GL098131

Chazette, P., David, C., Lefrère, J., Godin, S., Pelon, J., & Mégie, G. (1995). Comparative lidar study of the optical, geometrical, and dynamical properties of stratospheric post-volcanic aerosols, following the eruptions of El Chichon and Mount Pinatubo. *Journal of Geophysical Research: Atmospheres*, *100*(D11), 23195-23207. Retrieved from https://hal.archives-ouvertes.fr/hal-02902597 doi: 10.1029/95JD02268

Clerbaux, C., Boynard, A., Clarisse, L., George, M., Hadji-Lazaro, J., Herbin, H., … Coheur, P.-F. (2009). Monitoring of atmospheric composition using the thermal infrared IASI/MetOp sounder. *Atmospheric Chemistry and Physics*, *9*(16), 6041–6054. Retrieved from https://acp.copernicus.org/articles/9/6041/2009/ doi: 10.5194/acp-9-6041-2009

Da, C. (2015). Preliminary assessment of the Advanced Himawari Imager (AHI) measurement onboard Himawari-8 geostationary satellite. *Remote Sensing Letters*, *6*(8), 637-646. doi: 10.1080/2150704X.2015.1066522

Deshler, T., Johnson, B. J., & Rozier, W. R. (1993). Balloonborne measurements of Pinatubo aerosol during 1991 and 1992 at 41°N: Vertical profiles, size distribution, and volatility. *Geophysical Research Letters*, *20*(14), 1435-1438. Retrieved from https://agupubs.onlinelibrary.wiley.com/doi/abs/10.1029/93GL01337 doi: https://doi.org/10.1029/93GL01337

Dieudonné, E., Chazette, P., Marnas, F., Totems, J., & Shang, X. (2015). Lidar profiling of aerosol optical properties from Paris to Lake Baikal (Siberia). *Atmospheric Chemistry and Physics*, *15*(9), 5007–5026. Retrieved from https://acp.copernicus.org/articles/15/5007/2015/ doi: 10.5194/acp-15-5007-2015

Duflot, V., Baray, J.-L., Payen, G., Marquestaut, N., Posny, F., Metzger, J.-M., … Cammas, J.-P. (2017). Tropospheric ozone profiles by DIAL at Maïdo Observatory (Reunion Island): system description, instrumental performance and result comparison with ozone external data set. *Atmospheric Measurement Techniques*, *10*(9), 3359–3373. Retrieved from https://amt.copernicus.org/articles/10/3359/2017/ doi: 10.5194/amt-10-3359-2017

Eumetrain. (2020). *EUMeTrain Quick Guides.* Retrieved 2020-07-01, from http://www.eumetrain.org/rgb_quick_guides

Klett, J. D. (1985, Jun). Lidar inversion with variable backscatter/extinction ratios. *Appl. Opt.*, *24*(11), 1638–1643. Retrieved from http://opg.optica.org/ao/abstract.cfm?URI=ao-24-11-1638 doi: 10.1364/AO.24.001638

Kloss, C., Berthet, G., Sellitto, P., Ploeger, F., Taha, G., Tidiga, M., … Legras, B.

(2021). Stratospheric aerosol layer perturbation caused by the 2019 Raikoke and Ulawun eruptions and their radiative forcing. *Atmospheric Chemistry and Physics*, *21*(1), 535–560. Retrieved from https://acp.copernicus.org/articles/21/535/2021/ doi: 10.5194/acp-21-535-2021

Lurton, T., Jégou, F., Berthet, G., Renard, J.-B., Clarisse, L., Schmidt, A., ... Roberts, T. J. (2018). Model simulations of the chemical and aerosol microphysical evolution of the Sarychev Peak 2009 eruption cloud compared to in situ and satellite observations. *Atmospheric Chemistry and Physics*, *18*(5), 3223–3247. Retrieved from https://acp.copernicus.org/articles/18/3223/2018/ doi: 10.5194/acp-18-3223-2018

Prata, A. T., Young, S. A., Siems, S. T., & Manton, M. J. (2017). Lidar ratios of stratospheric volcanic ash and sulfate aerosols retrieved from CALIOP measurements. *Atmospheric Chemistry and Physics*, *17*(13), 8599–8618. Retrieved from https://acp.copernicus.org/articles/17/8599/2017/ doi: 10.5194/acp-17-8599-2017

Proud, S. R., Prata, A., & Schmauss, S. (2022). The January 2022 eruption of Hunga Tonga-Hunga Ha'apai volcano reached the mesosphere. *Earth and Space Science Open Archive*, 11. Retrieved from https://doi.org/10.1002/essoar.10511092.1 doi: 10.1002/essoar.10511092.1

Renard, J.-B., Dulac, F., Berthet, G., Lurton, T., Vignelles, D., Jégou, F., ... Daugeron, D. (2016). LOAC: a small aerosol optical counter/sizer for ground-based and balloon measurements of the size distribution and nature of atmospheric particles – Part 1: Principle of measurements and instrument evaluation. *Atmospheric Measurement Techniques*, *9*(4), 1721–1742. Retrieved from https://amt.copernicus.org/articles/9/1721/2016/ doi: 10.5194/amt-9-1721-2016

Renard, J.-B., Michoud, V., & Giacomoni, J. (2020). Vertical Profiles of Pollution Particle Concentrations in the Boundary Layer above Paris (France) from the Optical Aerosol Counter LOAC Onboard a Touristic Balloon. *Sensors*, *20*(4). Retrieved from https://www.mdpi.com/1424-8220/20/4/1111

Saunders, R., Hocking, J., Rundle, D., Rayer, P., Hayemann, S., Matricardi, A., ... Vidot, J. (2017). RTTOV-12 SCIENCE AND VALIDATION REPORT; Version : 1.0. *Doc ID : NWPSAF-MO-TV-41*(D2.2).

Sellitto, P., & Legras, B. (2016). Sensitivity of thermal infrared nadir instruments to the chemical and microphysical properties of UTLS secondary sulfate aerosols. *Atmospheric Measurement Techniques*, *9*(1), 115–132. Retrieved from https://amt.copernicus.org/articles/9/115/2016/ doi: 10.5194/amt-9-115-2016

Sellitto, P., Podglajen, A., Belhadji, R., Boichu, M., Carboni, E., Cuesta, J., ... Legras, B. (2022). The unexpected radiative impact of the Hunga Tonga eruption of January 15th, 2022, 18 April 2022. *PREPRINT (Version 1) available at Research Square*. doi: https://doi.org/10.21203/rs.3.rs-1562573/v1

Sellitto, P., Sèze, G., & Legras, B. (2017). Secondary sulphate aerosols and cirrus clouds detection with seviri during nabro volcano eruption. *International Journal of Remote Sensing*, *38*(20), 5657-5672. Retrieved from https://doi.org/10.1080/01431161.2017.1348635 doi: 10.1080/01431161.2017.1348635

Siddans, R. (2019). Water Vapour Climate Change Initiative (WV cci) Phase One, Deliverable 2.2; Version 1.0. *STFC Rutherford Appleton Laboratory (RAL)*(D2.2). Retrieved from https://climate.esa.int/documents/1337/Water_Vapour_CCI_D2.2_ATBD_Part2-IMS_L2_product_v1.0.pdf

Vernier, J.-P., Fairlie, T. D., Deshler, T., Natarajan, M., Knepp, T., Foster, K., ... Trepte, C. (2016). In situ and space-based observations of the Kelud volcanic plume: The persistence of ash in the lower stratosphere. *Journal of Geophysical Research: Atmospheres*, *121*(18), 11,104-11,118. Retrieved from https://agupubs.onlinelibrary.wiley.com/doi/abs/10.1002/2016JD025344 doi:

10.1002/2016JD025344

Witze, A. (2022). Why the Tongan eruption will go down in the history of volcanology. *Nature*(602), 376-378. doi: https://doi.org/10.1038/d41586-022-00394-y

Wylie, J. J., Voight, B., & Whitehead, J. A. (1999). Instability of Magma Flow from Volatile-Dependent Viscosity. *Science*, *285*(5435), 1883-1885. Retrieved from https://www.science.org/doi/abs/10.1126/science.285.5435.1883 doi: 10.1126/science.285.5435.1883

Yuen, D. A., Scruggs, M. A., Spera, F. J., Zheng, Y., Hu, H., McNutt, S. R., ... Tanioka, Y. (2022). Under the surface: Pressure-induced planetary-scale waves, volcanic lightning, and gaseous clouds caused by the submarine eruption of Hunga Tonga-Hunga Ha'apai volcano. *Earthquake Research Advances*, 100134. Retrieved from https://www.sciencedirect.com/science/article/pii/S2772467022000227 doi: https://doi.org/10.1016/j.eqrea.2022.100134

Zhu, Y., Toon, O. B., Kinnison, D., Harvey, V. L., Mills, M. J., Bardeen, C. G., ... Jégou, F. (2018). Stratospheric Aerosols, Polar Stratospheric Clouds, and Polar Ozone Depletion After the Mount Calbuco Eruption in 2015. *Journal of Geophysical Research: Atmospheres*, *123*(21), 12,308-12,331. Retrieved from https://agupubs.onlinelibrary.wiley.com/doi/abs/10.1029/2018JD028974 doi: https://doi.org/10.1029/2018JD028974

Supporting Information for "Aerosol characterization of the stratospheric plume from the volcanic eruption at Hunga Tonga January 15^{th} 2022"

Corinna Kloss [1], Pasquale Sellitto [2,3], Jean-Baptiste Renard [1], Alexandre Baron [4], Nelson Bègue [4], Bernard Legras [5], Gwenaël Berthet [1], Emmanuel Briaud [1], Elisa Carboni [6], Clair Duchamp [5], Valentin Duflot [4], Patrick Jacquet [1], Nicolas Marquestaut [7], Jean-Marc Metzger [7], Guillaume Payen [7], Marion Ranaivombola [4], Tjarda Roberts [1], Richard Siddans [6], Fabrice Jégou [1]

[1]Laboratoire de Physique et Chimie de l'Environnement et de l'Espace, CNRS/Université d'Orléans, UMR 7328

[2]Univ. Paris Est Créteil and Université de Paris-Cité, CNRS, Laboratoire Interuniversitaire des Systèmes Atmosphériques (LISA-IPSL), Institut Pierre Simon Laplace

[3]Istituto Nazionale di Geofisica e Vulcanologia, Osservatorio Etneo

[4]Laboratoire de l'Atmosphère et des Cyclones (LACy, UMR 8105 CNRS, Université de la Réunion, Météo-France), Université de La Réunion

[5]Laboratoire de Météorologie Dynamique, ENS-PSL/ Sorbonne Université/ École Polytechnique, UMR CNRS 8539

[6]UK Research and Innovation, Science and Technology Facilities Council, Rutherford Appleton Laboratory

[7]Observatoire des Sciences de l'Univers de La Réunion, UAR 3365 (CNRS, Université de La Réunion, Météo-France)

[1]Orléans, France

[2]Créteil, France

[3]Catania, Italy

[4]97400 Saint-Denis de La Réunion, France

[5]Paris, France

[6]Chilton, UK

[7]97490, Saint-Denis de La Réunion, France

Contents of this file

1. Text S1 to Movie S1 MSG-1: MSG-1 is one of the operational Meteosat Second Generation (MSG, designed and produced by ESA) geostationary satellites located at 45°E. It provides detailed imageries of the Earth since January 2004. In this study, we use the operational Eumetrain Ash RGB recipe to distinguish between clouds, SO_2 and ash signals. It uses the brightness temperatures (BT in K) of the three channels: 8.5, 10.4 and 12.3 256 μm. The recipe for the three color indexes ranging from 0 to 1 is R = (BT(12.3) - BT(10.4) + 257 4)/6, G = (BT(10.4) - BT(0.85) +4)/9, B = (BT(10.4) - 243)/60

2. Movie S1 An animation of MSG-1 brightnes temperature observations (Da, 2015) with the Eumetrain RGB recipe (Eumetrain, 2020).

3. Text S2 to Figure S2 OMPS: The Ozone Mapping Profiler Suite Limb Profiler (OMPS-LP) onboard the Suomi National Polar-orbiting Partnership satellite provides aerosol extinction and ozone observations since October 2011. Here, we use the aerosol extinction measurements version 2.0 at 745 nm and the integrated stratospheric Aerosol Optical Depth (Taha et al., 2021) together with the respectively provided tropopause altitude (from MERRA-2, e.g. (Gelaro et al., 2017).

4. Text S3 to Figure S3 CALIOP/CALIPSO: The Cloud-Aerosol Lidar with Orthogonal Polarisation (CALIOP) instrument onboard the Cloud-Aerosol Lidar and Infrared Pathfinder Satellite Observation (CALIPSO) satellite measures attenuated backscatter profiles at 532 nm. During 20-25 January CALIOP did not provide observations because of the solar activity. Here, we use observations along one orbit in Figure S3, supporting LOAC observations from 26/01.

5. Figure S2

Figure S1-S3 below

References

Da, C. (2015). Preliminary assessment of the Advanced Himawari Imager (AHI) measurement onboard Himawari-8 geostationary satellite. *Remote Sensing Letters*, *6*(8), 637-646. doi: 10.1080/2150704X.2015.1066522

Eumetrain. (2020). *EUMeTrain Quick Guides.* Retrieved 2020-07-01, from `http://www.eumetrain.org/rgb_quick_guides`

Gelaro, R., McCarty, W., Suárez, M. J., Todling, R., Molod, A., Takacs, L., … Zhao, B. (2017). The Modern-Era Retrospective Analysis for Research and Applications, Version 2 (MERRA-2). *Journal of Climate*, *30*(14), 5419 - 5454. Retrieved from `https://journals.ametsoc.org/view/journals/clim/30/14/jcli-d-16-0758.1.xml` doi: 10.1175/JCLI-D-16-0758.1

Taha, G., Loughman, R., Zhu, T., Thomason, L., Kar, J., Rieger, L., & Bourassa, A. (2021). OMPS LP Version 2.0 multi-wavelength aerosol extinction coefficient retrieval algorithm. *Atmospheric Measurement Techniques*, *14*(2), 1015–1036. Retrieved from `https://amt.copernicus.org/articles/14/1015/2021/` doi:

10.5194/amt-14-1015-2021

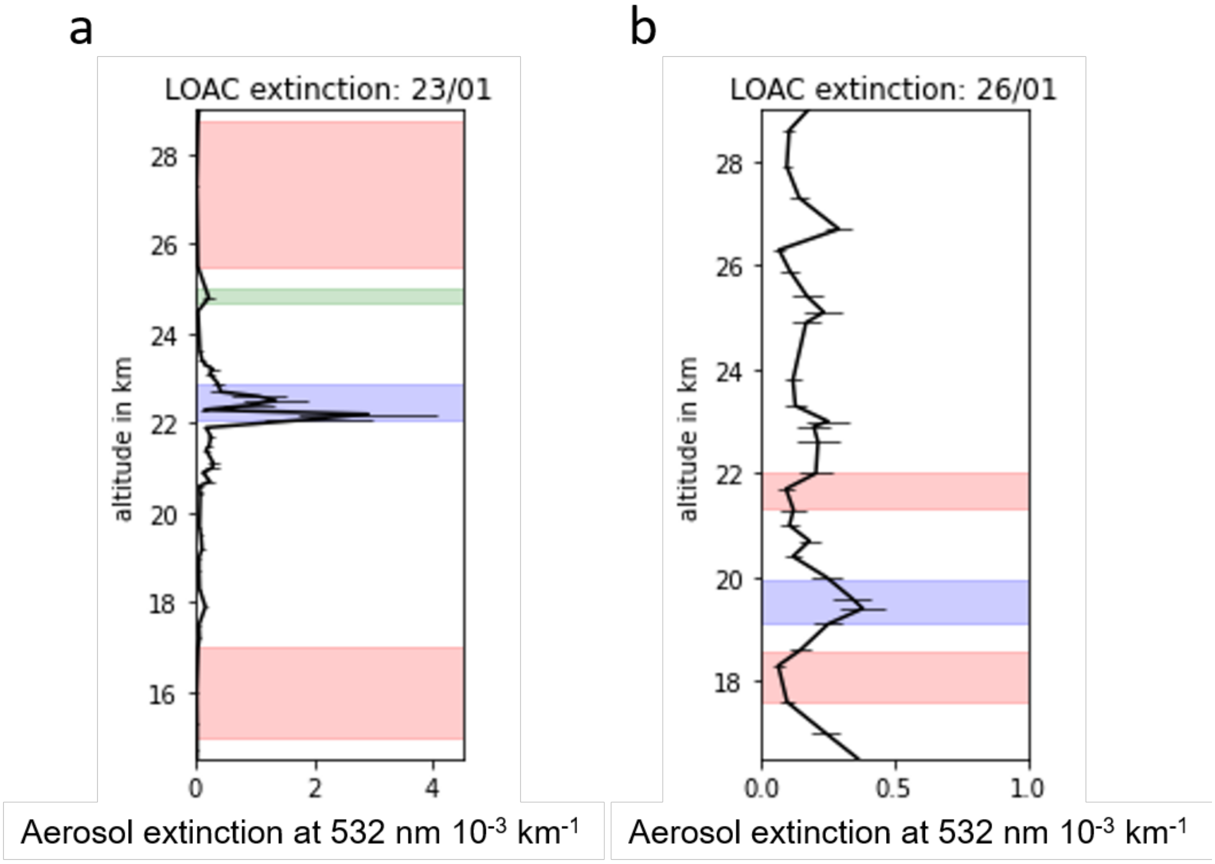

Figure S1. Aerosol extinction values derived from LOAC observations with selected plume and background altitude ranges as presented on the right side of Figure 2.

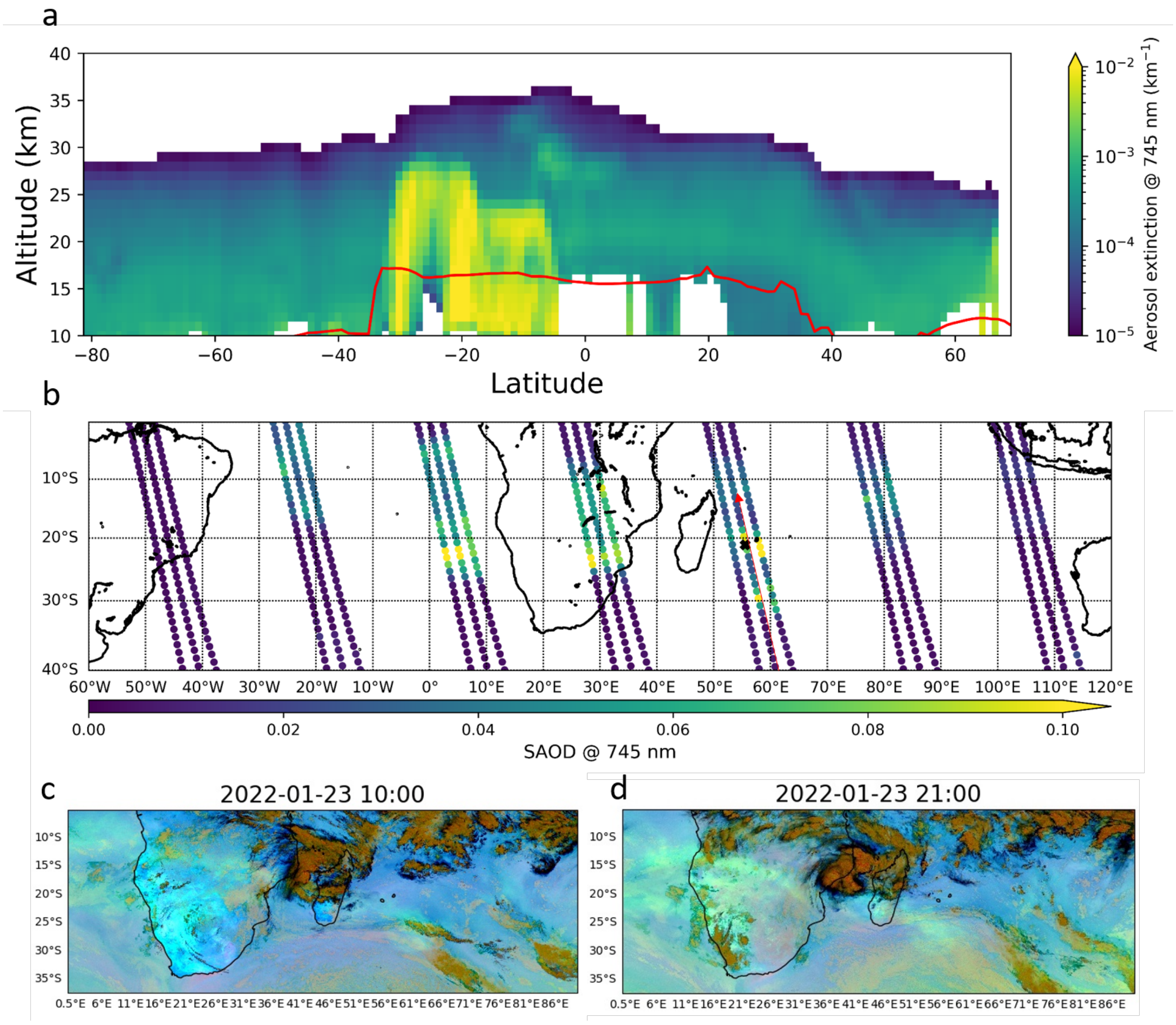

Figure S2. (a) OMPS aerosol extinction curtain plot at 745 nm (center slit) according to the observational track as indicated in (b) on 23/01 (measurements at La Réunion at around 10:00 UTC). The red line in (a) represents the tropopause altitude. (b) respective stratospheric AOD values. (c) and (d) show the horizontal plume distribution with the MSG-1 RGB recipe, at the time of the OMPS overpass in (c) and at 21:00 UTC during the time of the LOAC observations (20:04-21:35 UTC) (d).

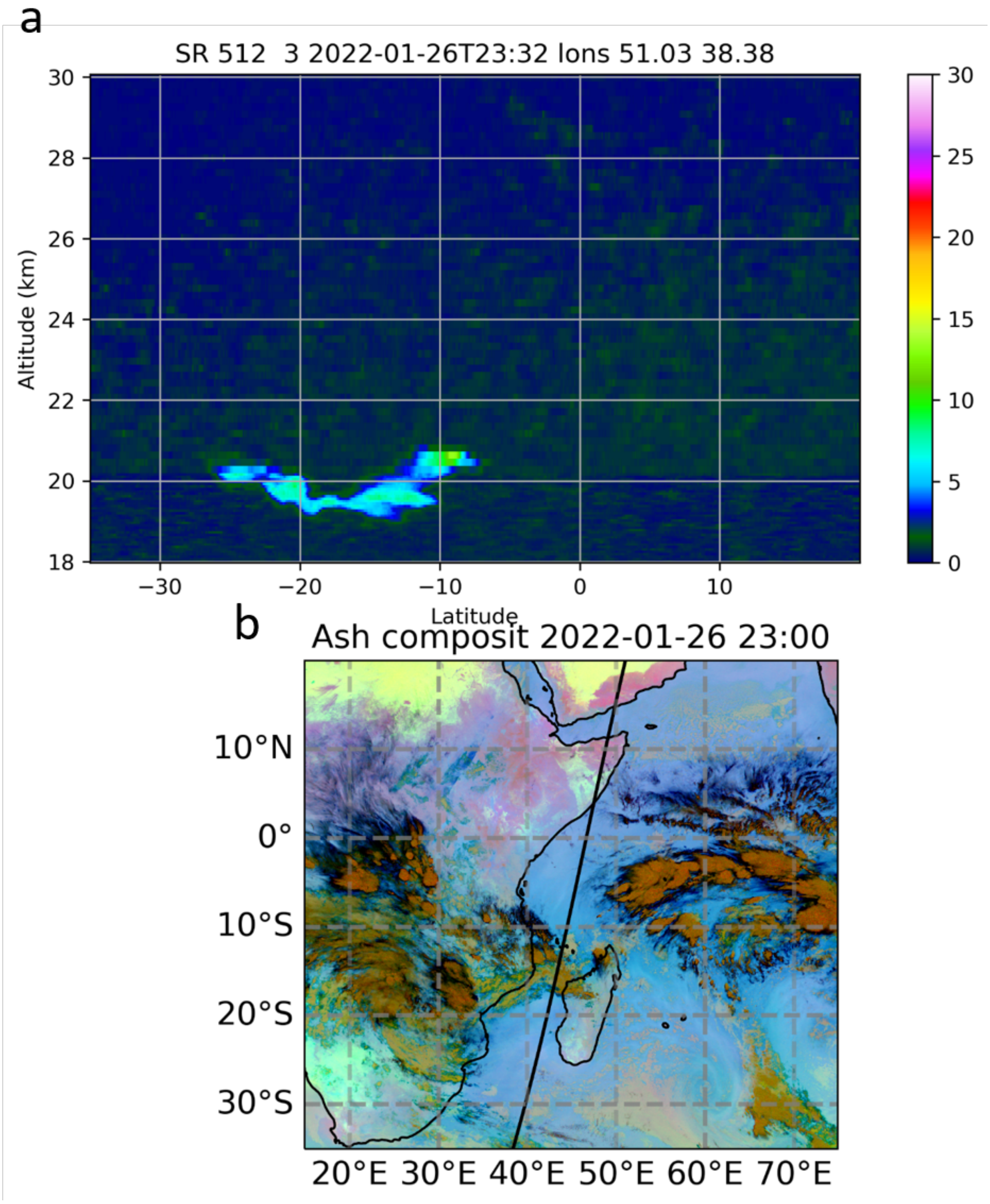

Figure S3. (a) CALIOP aerosol 532 nm backscatter ratio observations along the orbit track (orbit: 2022-01-26T23_03_33ZN) as indicated in (b). (b) The respective MSG-1 (with RGB recipe) observations during the CALIOP overpass.